Phase-space density in the magneto-optical trap

C. G. Townsend, N. H. Edwards, C. J. Cooper, K. P. Zetie, and C. J. Foot
Clarendon Laboratory, Parks Road, Oxford OX1 3PU, England

A. M. Steane,* P. Szriftgiser, H. Perrin, and J. Dalibard
Laboratoire Kastler Brossel, Unité de Recherche de l'Ecole Normale Supérieure et de l'Université Pierre et Marie Curie, associée au CNRS, 24 rue Lhomond, F-75231 Paris CEDEX 05, France

(Received 24 April 1995)

We present an investigation of the cesium magneto-optical trap, with particular regard to the best combination of atomic density and temperature that can be produced. Conditions in the trap depend on four independent parameters: the detuning and intensity of the light, the gradient of the magnetic field, and the number of atoms trapped. We have varied all these parameters and measured the temperature and density distribution of the trapped cloud. Both the nonlinear variation with position of the restoring force and the reabsorption of photons scattered in the cloud limit the maximum density, and we present an empirical model that takes this into account. This in turn limits the density in phase space ρ (defined as the number of atoms in a box with sides of one thermal de Broglie wavelength). We have observed a maximum $\rho = (1.5 \pm 0.5) \times 10^{-5}$, with a spatial density of about 2×10^{11} atoms/cm^3.

PACS number(s): 32.80.Pj

I. INTRODUCTION

The magneto-optical trap (MOT) is now widely used as a convenient source of cold, dense clouds of atoms such as alkali metals and noble gases. Much work has been done to determine the limitations on the cooling one can obtain in the MOT. The restrictions on the compression have also been studied, but less thoroughly. This paper describes a detailed experimental study of the MOT, with the aim of discovering the best possible combination of temperature and density that can be attained; in other words, the maximum *phase-space density* of the trapped atoms. In pursuing this aim, we found that a number of separate processes combine to produce the limitations on the phase-space density. We present a model that generalizes existing treatments of the MOT in order to embrace a wide range of its behavior.

The MOT consists of a combination of four or more laser traveling waves and a quadrupole magnetic field [1]. The most common geometry is six laser beams arranged to form three mutually perpendicular standing waves, intersecting at the zero of the magnetic field; this is the geometry assumed throughout this paper.

The first experiments were interpreted using a "Doppler" model of the MOT [1], in which the force on a trapped atom arises from the imbalance in radiation pressure forces in each of the three pairs of laser beams, these imbalances arising from the Doppler and Zeeman shifts of the beam frequencies in the rest frame of the atom. This type of model is acceptable for atoms in the process of being captured by the trap, but does not describe the important region at the center of the trap where the captured atoms settle. Here, the dominant force on the atom is caused by the "sub-Doppler" mechanisms that occur in polarization gradients, and involves a complicated combination of optical pumping and atomic-state-dependent transition rates [2].

In the case of low spatial density of trapped atoms, a qualitative understanding of the MOT has been obtained theoretically [3,4], and experimental measurements are used to obtain quantitative results [3–7]. Scaling laws for some of the properties, such as the temperature and radius of the trapped cloud, have been obtained from simple theoretical descriptions and these laws are found to predict fairly well the trends observed in practice. In this way one can construct semiempirical formulas for the various parameters of the trap, using experimental results to supply the proportionality factors. However, there is still some uncertainty in the literature as to the correct values of fundamental parameters such as the spring constant at the center of a MOT, so we have addressed this in our own work.

One only obtains the low-density regime in practice if one takes pains to produce it. In normal operation the MOT is not a system of independent particles, since interactions between the trapped atoms are important. The most significant of these are the reabsorption of scattered photons ("multiple scattering") and collisions between trapped atoms in which the internal state of one of the collision partners changes ("cold collisions"). With the effects of polarization gradients, multiple scattering, and cold collisions, the MOT is a very complicated system, and it is extremely difficult to construct a complete theoretical model from first principles [8]. In such a situation, we rely on the technique just described, that of

*Present address: Clarendon Laboratory, Parks Road, Oxford OX1 3PU, England.

combining simple theories with experimental results to produce a set of semiempirical formulas describing the MOT [9]. Such a set of formulas is presented in this paper.

Attaining the highest possible phase-space densities in a MOT is an important step towards the observation of collective quantum effects such as Bose-Einstein condensation. For an atom of mass M the "thermal de Broglie wavelength" Λ is defined by

$$\Lambda = \frac{\hbar\sqrt{2\pi}}{\sqrt{Mk_BT}}, \tag{1}$$

where $\hbar$ is Planck's constant divided by 2π and k_B is the Boltzman constant. If n is the spatial density of atoms, then we define the "density in phase space" as the dimensionless quantity

$$\rho = n\Lambda^3. \tag{2}$$

This can be considered, roughly, as the number of particles in a box of size $\hbar^3$ in phase space. For spin-zero particles confined in a box, Bose-Einstein condensation occurs when $\rho = 2.612$.

A promising route to achieving the necessary compression and cooling is to load a conservative trap (such as a magnetic, dipole-force, or gravitational trap) and then perform evaporative cooling. The value of the final phase-space density obtainable after evaporative cooling usually increases as a function of its value before cooling, so it is important to start from the highest possible initial value. In work with laser-cooled atoms, the MOT may be used to provide this initial condition to start the evaporative cooling process.

A recently proposed method to increase the phase-space density of atoms on a MOT is the so-called "dark" MOT introduced by Ketterle *et al.* [10] (see also Anderson *et al.* [11]), in which the unwanted effects of multiple scattering are reduced by shelving most of the trapped atoms in a long-lived state that is only weakly coupled to the trapping light field. The regime where the normal MOT reaches its highest phase-space density is also one where multiple scattering is much reduced, so there is no reason *a priori* that the normal MOT should not produce phase-space densities as high as those possible in the dark MOT.

A general introduction to the magneto-optical trap is provided by Steane, Chowdhury, and Foot [3]. Drewsen *et al.* [4] provide precise calculations in one dimension as well as many useful measurements on a cesium MOT. Wallace *et al.* [5] and Kohns *et al.* [6] describe measurements for trapped rubidium. Other works on more specific aspects of the MOT will be referred to as they arise in our own discussion.

This paper is organized as follows. In Sec. II we describe our model of the MOT, which includes various different regimes of behavior. This model assumes a steady-state operation of the MOT. In Sec. III we consider the possibility of increasing the phase-space density in a transient way by suddenly changing the parameters of the MOT (laser detuning, intensity, magnetic field gradient). Section IV describes our experimental investigations and results.

Our experiments using cesium atoms confirm the general features of our model of the trap and supply the required empirical factors. The main results are as follows. We provide measurements of the temperature in optical molasses (equal to that in a low-density MOT [4,5,12]), showing agreement with a previous study [4]. Difficulties arising in measurements of the spring constant at the center of the trap are discussed, and our own measured values reported. Our model takes into account the spatial capture range of the strong restoring force at the center of the MOT; the trapped cloud can easily extend beyond this range. Measurements of this capture range are reported, showing reasonable agreement with our simple model. Observations of the atomic density and velocity distributions in a cloud extending beyond the capture region of the confining force are also reported for the first time. Finally, we provide a set of measurements of the density n in the MOT and consider the limitations on the phase-space density ρ. It is known that the presence of many atoms in a MOT leads to an increase in both the volume and the temperature of the trapped cloud. Our results show that ρ is limited primarily through the volume rather than the temperature. Densities up to 2.5×10^{11} atoms per cm^3 were observed, and the maximum phase-space density was $\rho = (1.5 \pm 0.5) \times 10^{-5}$. We find that the density in the trap scales with laser detuning δ and Rabi frequency Ω roughly as $n \propto \delta^{0.4}\Omega^{-1}$, which is much slower than the variation one expects from a simple theory. The breakdown of the MOT at low light shifts is also apparent in our results and is discussed.

II. THE STATIC MOT

In this section, we consider the MOT in a steady state. That is, a dynamic equilibrium between capture and loss processes maintains a fixed number of atoms. We assume that heating can be modeled by a single momentum diffusion constant D, and confinement and damping by a force $\mathbf{f}$. We suppose a basic trapping and damping force $\mathbf{f}^0(\mathbf{r},\mathbf{v})$, which is present even when only one atom is trapped, plus a force $\mathbf{f}^{aa}(\mathbf{r},\mathbf{v},n)$ arising from the influence of other atoms on the local radiation field:

$$\mathbf{f}(\mathbf{r},\mathbf{v},n) = \mathbf{f}^0(\mathbf{r},\mathbf{v}) + \mathbf{f}^{aa}(\mathbf{r},\mathbf{v},n). \tag{3}$$

These forces are averaged over a box with sides of one wavelength. It is usual to consider the motion close to the origin (the center of the trap) and at low velocities, and assume a linear dependence of $\mathbf{f}^0$ on $\mathbf{r}$ and $\mathbf{v}$ (a damped harmonic oscillator model). However, the nonlinearity of the force as a function of $\mathbf{r}$ is an important feature of the MOT and will be taken into account in our discussion. In order to avoid building into our model too many assumptions about the variation of $\mathbf{f}^0$ with $\mathbf{r}$ and $\mathbf{v}$, we define the spring constant tensor κ_{ij} as the negative of the gradient of the force at the origin,

$$\kappa_{ij} = -\left\langle \frac{\partial f_i^0}{\partial r_j} \right\rangle, \tag{4}$$

where the derivative is evaluated at $r = 0$, and the angle brackets denote an average over the velocity distribution of the atoms in the central part of the trap (the "central part" will be defined more precisely later). The axes $i = \{x, y, z\}$ are chosen along the laser beams, and the axis of the magnetic field coils is along z (Fig. 3). One expects κ_{ii} to be proportional to the magnetic field gradient, leading to the anisotropic form $\kappa_{xx} = \kappa_{yy} = \kappa_{zz}/2$ in a magnetic quadrupole field.

We do not propose any particular model for friction and diffusion in the trap. We assume merely that in a steady state (still supposing $\mathbf{f}^{aa}$ to be negligible), the standard deviations $\{\Delta r, \Delta v\}$ of the velocity and position distributions are linked through

$$\frac{1}{2}M\Delta v_i^2 = \frac{1}{2}\kappa_{ii}\Delta r_i^2. \tag{5}$$

This equation is modeled on the equipartition theorem. This theorem cannot be applied directly to the trapped cloud of atoms, since the cloud is not an isolated system in thermal equilibrium, but (5) is found to be useful in practice in a wide range of conditions. Our experimental measurements of κ are, in fact, measurements of the ratio $M\Delta v^2/\Delta r^2$, so the assumption we make is that the κ appearing in Eq. (5) is the same as the κ appearing in Eq. (4). Care must be taken to be sure that experimental conditions are such that this assumption is valid (that is, $\mathbf{f}^{aa}$ and higher-order terms of $\mathbf{f}^0(r, 0)$ are both negligible).

The "interatomic" force $\mathbf{f}^{aa}$ is a shorthand for the change in the local radiation force on a given atom, brought about by the presence of all the other atoms in the trap which influence the local radiation field [13,14]. The main influence they have is to extract photons from, and change the phase of, the incident laser field, and to create a "background field" of scattered photons [8,15,16]. This has complicated effects on the small-scale structure of the cloud [17], which we will not attempt to model. However, for the large-scale properties such as the average density and temperature of the cloud, the net effect can be roughly modeled as a change in κ combined with a repulsive photon pressure between atoms [14], and this is the model we will discuss in Sec. II B below.

Throughout, the discussion is not intended to be precise in detail but to give a description that will enable most properties of the trap to be derived to within 50% accuracy. As we will show, the behavior of the trap can be divided broadly into four regimes. At small numbers of trapped atoms (typically less than 10^4), the density is low and multiple scattering effects are insignificant. We call this first regime "temperature limited," since the volume of the trapped cloud depends on its temperature; this is discussed in Sec. II A. At higher numbers of trapped atoms, we reach the multiple scattering regime discussed in Sec. II B. At still higher numbers of trapped atoms, or at low light shifts and high field gradients, the nonlinearity of the spatial dependence of the trapping force is important, and the trap enters a "two-component" regime, discussed in Sec. II C. Finally, when there are many atoms in the trap, and the detuning is not too large, the trapped cloud of atoms becomes optically thick. This is not taken into account in our empirical model, and represents a fourth regime (discussed in [9]) which we have chosen not to investigate.

In discussing the magneto-optical trap, we will use δ for the absolute value of the detuning $|\omega_L - \omega_0|$ of the laser frequency with respect to the atomic resonance frequency. (All our experiments use "red" detunings, $\omega_L < \omega_0$.) The natural linewidth of the atomic excited state $6P_{3/2}$ is $\Gamma = 2\pi \times (5.22 \pm 0.01)$ MHz for cesium [18], and the Rabi frequency Ω in a light field of intensity I is

$$\Omega = \Gamma\sqrt{I/2I_S}, \tag{6}$$

where

$$I_S = \frac{4\pi^2\hbar c\Gamma}{6\lambda^3} \tag{7}$$

and c is the speed of light. The saturation intensity $I_S = 1.1\,\mathrm{mW/cm^2}$ for the transition $6S_{1/2}F = 4, M_F = 4 \rightarrow 6P_{3/2}F = 5, M_F = 5$ in cesium. Throughout this paper, Ω will refer to the Rabi frequency of a *single* laser beam; the total Rabi frequency of all six laser beams in the trap is denoted by Ω_{tot}.

A. Temperature limited regime

At small numbers of atoms, the atomic density is low and interatom effects can be neglected: the trapped gas acts as a collection of N independent atoms. In this regime, the atomic spatial and momentum distributions are close to Gaussian and can be characterized by three radii r_x, r_y, r_z and a temperature T. The radius along each axis ($i = x, y, z$) is given by the equipartition theorem [cf. Eq. (5)]

$$\frac{1}{2}\kappa_{ii}r_{i,T}^2 = \frac{1}{2}k_BT. \tag{8}$$

The subscript T on r is to emphasize that the radius is limited by the temperature of the cloud. At the center of a quadrupole magnetic field formed by two coils, the field gradient along the coil axis (the z direction) is twice that along the x or y axes, so that $\kappa \equiv \kappa_z = 2\kappa_x = 2\kappa_y$, since κ is proportional to the field gradient. This means $r \equiv r_z = r_x/\sqrt{2} = r_y/\sqrt{2}$, since the temperature is assumed to be isotropic. With N atoms, the peak spatial atomic density (at the center of the elliptical Gaussian distribution) is

$$n = \frac{N}{2\left(\sqrt{2\pi}\,r_T\right)^3}. \tag{9}$$

Note that since the temperature does not depend on the number of trapped atoms, the cloud radius is independent of N and thus the density is proportional to N. This is not the case in the other regimes discussed below. In terms of N, κ, and T, the phase-space density is

$$\rho = \frac{N\hbar^3}{2k_B^3T^3}\left(\frac{\kappa}{M}\right)^{3/2}. \tag{10}$$

Since we are interested in obtaining high phase-space densities, we consider the case of low temperatures: these

TABLE I. Reported κ measurements, converted into values for κ_0. The final two rows give the results of a semiclassical, three-dimensional numerical calculation for an idealized atom having parameters (such as the wave vector) appropriate for cesium.

Value of κ_0 (10^{-19} N/m)	Atom	Transition	Method	Reference
0.4	Cs	$4 \rightarrow 5$	measured r & T	[4] Fig. 14
1	Cs	$4 \rightarrow 5$	measured r & T with few atoms	[4] Table I
0.5	Cs	$4 \rightarrow 5$	imposed oscillating B field	[7]
2.7	Cs	$4 \rightarrow 5$	beam imbalance	[3]
0.2	^{85}Rb	$3 \rightarrow 4$	imposed oscillating B field	[6]
2.5	^{85}Rb	$3 \rightarrow 4$	measured r & T; beam imbalance	[5]
2.0	^{87}Rb	$2 \rightarrow 3$	measured r & T; beam imbalance	[5]
3.0	'Cs'	$1 \rightarrow 2$	numerical calculation	[26]
3.3	'Cs'	$4 \rightarrow 5$	numerical calculation	[26]

are produced in the MOT when the saturation of the atomic transition by the laser light is small. In this regime, the spring constant κ arises from optical pumping among the Zeeman sublevels of the ground state, which produces a difference in the scattering rates of photons from one laser beam compared with another. A one-dimensional semiclassical analysis [3,12] then shows that κ is independent of laser intensity and inversely proportional to detuning for $\delta > 2\Gamma$. It can therefore be written

$$\kappa = \kappa_0 \frac{\Gamma}{\delta} \frac{b}{b_0} \qquad (\text{for } \delta > 2\Gamma), \tag{11}$$

where $b = dB/dz$ is the gradient of the magnetic field, κ_0 is a constant of proportionality, and we will take $b_0 = 1\,\text{G/cm}$. A quantum analysis performed in one dimension [4] confirms this prediction. We will discuss later the way in which this equation breaks down at very low light shifts (high detuning and low Rabi frequency). Measurements on three-dimensional traps appear to be in agreement with this overall dependence, although κ is difficult to measure, since it is hard to retain a measurable signal while being sure that the trap is in the simple temperature-limited regime and in the linear region of the confining force.

Assuming that Eq. (11) does indeed apply in three-dimensions (3D), the reported measurements of κ can be converted into measurements of κ_0 as shown in Table I.[1] There is a wide variation in these values. One should resist the temptation to take an average of the values in Table I — it is possible that any one experiment is in fact more precise than the average of all the others put together. Suffice it to say that experimental knowledge of κ remains somewhat problematic.

An early work [12] showed that the temperature in a cesium magneto-optical trap at low atomic density is similar to that in the corresponding molasses, i.e., to that obtained in the same physical system but with zero field gradient. More recently, two studies [4,5] have shown that the temperature in the MOT is indeed exactly the same as that in a molasses of the same laser-field configuration (for low atomic density and field gradients of order 10 G/cm). For detunings larger than a few linewidths and light shifts in the range indicated, the temperature is expected to vary as

$$k_B T = C_0 + C_\sigma \hbar \frac{\Omega^2}{\delta}$$

$$(\delta \geq 5\Gamma,\ 0.02\Gamma < \Omega^2/\delta < 0.4\Gamma). \tag{12}$$

This expectation was originally based on measurements [20] and numerical analysis [21] of an optical molasses with linearly polarized beams. The recent studies [4,5] confirmed this behavior for circularly polarized light.

We have made many measurements of the temperature in the molasses obtained after the magnetic quadrupole field of a MOT is switched off, which we describe in the experiment section of this paper. The results are reproduced here in order to use them to build our semiempirical model. We observe a slight departure from a linear dependence on the light shift, for values of $\Omega^2/\Gamma\delta$ between 0.05 and 0.4. However, we can nevertheless fit a straight line through all our data having $0.05 < \Omega^2/\Gamma\delta < 0.4$ (i.e., temperatures up to about $30\,\mu$K), to obtain $C_0/k_B = 1 \pm 0.5\,\mu$K, $C_\sigma = 0.28 \pm 0.05$. In the following this pair of values for C_0 and C_σ is used.

When the constant term in (12) can be neglected, $T \propto \Omega^2/\delta$, leading to a cloud radius independent of detuning as well as number, and proportional to the Rabi frequency [3,4]

$$r_T = \sqrt{\frac{\hbar C_\sigma \Gamma}{\kappa_0}} \frac{\Omega}{\Gamma} \sqrt{\frac{b_0}{b}}. \tag{13}$$

B. Multiple scattering regime

With a medium number of atoms in the trap (typically above 10^4), reabsorption of scattered photons within the

[1]Note that in Ref. [4], the cloud radius at one standard deviation, σ, is correctly included in Eq. (29), but erroneously described in the text as the "$1/e$ radius;" the latter should read "$1/\sqrt{e}$ radius" [19].

trapped cloud is an important effect. The restoring force and friction are still produced by sub-Doppler mechanisms, as for the case of a small number of atoms, but these mechanisms are themselves modified. No simple model for this situation is presented in this paper. Instead, we use an empirical scaling law for the density in the trap, which we find to vary for detunings above a few linewidths approximately as $n_{\rm MS} \propto b\,\delta^{0.5}\,\Omega^{-1}$:

$$n_{\rm MS} = C_{\rm MS}\,\frac{\kappa_0}{\lambda\hbar\Gamma}\,\frac{b}{b_0}\left(\frac{\delta\Gamma}{\Omega^2}\right)^{1/2} \quad (\delta > 2\Gamma). \tag{14}$$

Here, $C_{\rm MS}$ is a dimensionless parameter whose value is given by experiment (our experimental measurements give a value of order $C_{\rm MS} \simeq 50$). The parameter κ_0 is included in Eq. (14) because we expect that if the MOT has a large spring constant in the temperature-limited regime, then it will produce proportionately large densities in the multiple scattering regime. However, we do not make any particular assumptions concerning the scaling of the spring constant in the multiple scattering regime other than that it is proportional to the magnetic field gradient.

We find experimentally that the density in the multiple scattering regime is almost independent of the number of atoms trapped. Walker, Sesko, and Wieman [13] originally observed this, and proposed a simple model in which the restoring force remained simple harmonic, but with an additional inverse-square law repulsive force between atoms. Using Gauss's theorem, it is easy to show [14] that this leads to a uniform density distribution in the trapped cloud, which grows in volume as more atoms are added, maintaining a constant density independent of the number. The repulsive interatomic force arises from reabsorption of scattered photons in the cloud and, according to this model, the density is given by [14]

$$n_{\rm MS} = \frac{3\kappa c}{I_{\rm tot}\sigma_L^2\,(\sigma_R/\sigma_L - 1)}. \tag{15}$$

Here, $I_{\rm tot} = 2I_S\Omega_{\rm tot}^2/\Gamma^2$ is the *total* light intensity due to the six trapping beams (averaged over a wavelength-sized box), σ_L is the optical cross section for absorbing photons from the laser field, and σ_R is the optical cross section for absorbing photons reradiated from atoms in the trapped cloud. Using a two-level model for the atom, the expression for σ_L is

$$\sigma_L = \frac{3\lambda^2}{2\pi}\,\frac{\Gamma^2/4}{\delta^2 + \Gamma^2/4 + \Omega_{\rm tot}^2/2}. \tag{16}$$

The calculation of σ_R is more involved: it was performed numerically in [14] and approximated analytically in [3]. To improve on the calculation in [3] we proceed as follows. We consider a two-level atom illuminated by a single traveling wave and deduce the fluorescence spectrum in the limit $\Omega_{\rm tot},\ \delta \gg \Gamma$ using the dressed atom approach [22]. This leads to a complicated expression for σ_R, which can be fitted, to within 30% accuracy, by the formula

$$\frac{\sigma_R}{\sigma_L} - 1 = \frac{\Omega_{\rm tot}^2}{2\,\Gamma^2}\,\frac{\delta^2 - 2\,\Gamma^2}{\delta^2 + \Omega_{\rm tot}^2}. \tag{17}$$

Substituting this in Eq. (15), one may deduce the density in the MOT in the presence of multiple scattering of photons:

$$n_{\rm MS} \stackrel{?}{=} \kappa\,\frac{\left(4\delta^2 + \Gamma^2 + 12\,\Omega^2\right)^2}{18\lambda\hbar\Gamma\Omega^4}\left(\frac{\delta^2 + 6\,\Omega^2}{\delta^2 - 2\,\Gamma^2}\right), \tag{18}$$

$$\simeq \frac{8}{9}\,\frac{\kappa_0}{\lambda\hbar\Gamma}\,\frac{b}{b_0}\,\frac{\Gamma\delta^3}{\Omega^4}. \tag{19}$$

The question mark in Eq. (18) is there because our experimental results, described in later sections of this paper and summarized by the scaling law mentioned above, are not consistent with this equation. In other words, the relatively weak dependence of $n_{\rm MS}$ on δ and Ω that we observe is surprising. We do not have a good understanding of this, but suppose that it indicates that the simple model of multiple scattering is not a good guide to the real situation.

A difference between our observations and those in [14] is that we rarely observe a uniform distribution of density in the MOT in the multiple scattering regime. We have observed fairly uniform distributions when the detuning and magnetic field gradient are small, but for most parameter values the density distribution is well approximated by a Gaussian function. The signature of the multiple scattering regime is then not the spatial form of the density distribution in the trap, but the appearance of a maximum density that is almost independent of the number of atoms trapped.

If there are N atoms in the trapped cloud, then the limiting density $n_{\rm MS}$ dictates the cloud radius. Since the density is now proportional to b, one might expect a radius scaling as the cube root of b, which would imply that the ellipticity of the trapped cloud is reduced, compared with the temperature-limited regime. We assume that we can approximate the cloud as a spherical distribution with rms radius given by

$$r_{\rm MS} = \frac{1}{\sqrt{2\pi}}\left(\frac{N}{n_{\rm MS}}\right)^{1/3}. \tag{20}$$

This is to be compared with the radius r_T given by Eq. (8). These two radii define the boundary between the temperature-limited and multiple scattering regimes. When $r_{\rm MS} > r_T$, the cloud is not compressed to the temperature-limited radius but remains fatter due to the multiple photon scattering.

Figures 1(a) and 1(b) show "phase diagrams" for a MOT at $\delta = 4\,\Gamma$ and $\delta = 8\,\Gamma$, respectively, with $\Omega^2 = 0.5\,\Gamma^2$. Figures 1(c) and 1(d) show diagrams for the same conditions but higher laser intensity, $\Omega^2 = 2\,\Gamma^2$. We see that with 10^4 atoms, the trap is in the temperature-limited regime for most values of detuning and field gradient, while with 10^6 atoms it is mostly in the multiple scattering regime. The other delimiting lines in Fig. 1 will be explained in the next section.

Multiple scattering also causes the temperature of the atoms to be different from that predicted at low densities. Two studies have shown temperatures increasing in proportion to the cube root of the total number of trapped atoms [4,23]. This is due to an enhanced momentum dif-

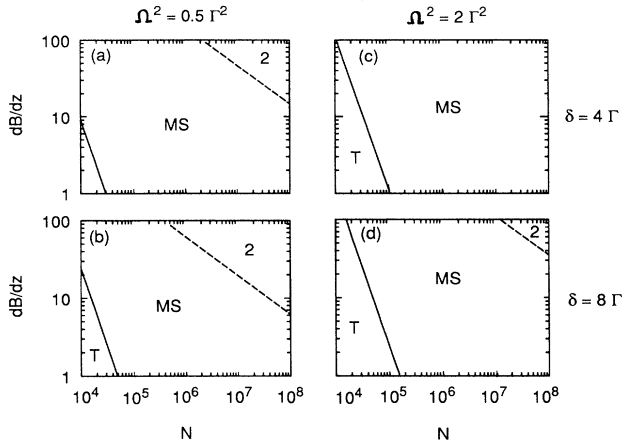

FIG. 1. Different regimes of behavior of a magneto-optical trap. The curves show the positions of the boundaries between the temperature-limited, multiple scattering, and two-component regimes, marked T, MS, and 2, respectively, on the diagrams. Each diagram (a)–(d) is for a different combination of Rabi frequency and detuning, as follows. $\{\Omega^2/\Gamma^2, \delta/\Gamma\}$ = (a) $\{0.5, 4\}$, (b) $\{0.5, 8\}$, (c) $\{2, 4\}$, (d) $\{2, 8\}$. The parameter values used are $\kappa_0 = 1 \times 10^{-19}$ N/m, $C_{\rm MS} = 50$, $C_l = 1.4$. The field gradient (on the y axis) is in units of G/cm.

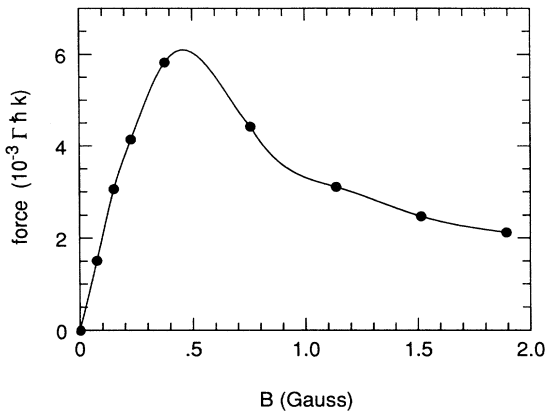

FIG. 2. Force on a stationary atom in a MOT, as given by a semiclassical numerical calculation. The points are calculated, the line is a spline fit to guide the eye. The calculation used $\delta = 6\,\Gamma$, $\Omega = 0.9\,\Gamma$ and was performed for a $J = 4 \rightarrow J = 5$ transition. Full details of the method will be published elsewhere [26]; the figure illustrates the general form of the variation of the force with magnetic field.

fusion and reduced friction caused by the multiple scattering [8,15,16], although a quantitative model remains to be worked out. We will show later that multiple scattering limits the density before it significantly raises the temperature, so we will not need to take this temperature rise into account in establishing the boundary between the temperature-limited and multiple scattering regimes.

To conclude this section, we note that the denominator in Eq. (18) goes to zero at $\delta = \sqrt{2}\,\Gamma$. For detunings below this value, the simple theory predicts that the presence of multiple scattering tends to *compress* rather than expand the cloud. This is because near $\delta = 0$ the sidebands in the Mollow triplet fluorescence spectrum are shifted *away* from the atomic resonance frequency so that the cross section for reabsorbing them is less than that for absorbing the nearly resonant laser light. One might expect this general argument to apply also in the real case of cesium atoms with multiple Zeeman sublevels, and a three-dimensional radiation field. We have looked for such a compression effect experimentally but found no sign of it.

C. Two-component regime

The restoring force in a MOT is not a linear function of position. The force gradient df/dz is high in a small region near the center of the trap and low outside this region [3]—see Fig. 2. The strong confinement in the small central region is due to the influence of the magnetic field on optical pumping between the Zeeman sublevels of the atomic ground state, while the weaker confinement in the rest of the trap is due to the Zeeman shifts of the various transitions to the excited state. As more and more atoms are loaded into the trap the cloud becomes fatter and fatter, until eventually it fills the central, strongly confining region. If further atoms are added the cloud then spills over into the weakly confining surrounding volume, spreading out to a much larger radius. With a sufficiently large number of atoms, almost all the atoms are in this large surrounding volume. When this happens the trap is essentially a simple "Doppler theory" system. The presence of polarization gradients in the laser field no longer determines the average temperature and density in the trap.

Semiclassical [24] and fully quantum-mechanical [25] calculations have shown that the boundary between the central and outer regions in a one-dimensional MOT occurs at a radius such that the Zeeman shift is of the same order as the light shift in the ground state. Preliminary results of calculations predict the same behavior in a 3D trap and yield a numerical value for the relevent radius:

$$\mu_B b\, r_l = C_l \frac{\hbar\Omega^2}{\delta}. \tag{21}$$

We choose to define r_l as the radius at which the restoring force reaches a local maximum — see Fig. 2. C_l is a constant proportionality factor. A semiclassical numerical calculation [26] for a $J = 4 \rightarrow 5$ atomic transition gives $C_l \simeq 0.9$. The calculation assumed the same Landé factor for the ground and excited states, which is not appropriate for cesium, but at low saturation the result is not expected to be sensitive to this.

The radius r_l allows us to define further boundaries on our phase diagram for the MOT (Fig. 1). When the radius of the trapped cloud reaches r_l, the MOT enters the two-component regime. The signature of this regime is a density distribution consisting of two components: a

diffuse Gaussian ball extending out to a large radius, with a small, much more dense clump in the center. The large diffuse ball is sensitive to imbalances in the intensities of the trapping beams, while the central clump is not [3]. The boundary $r_{\rm MS} = r_l$ defines the transition between the multiple scattering and two-component regimes. In thus defining the boundary, we recognize that $r_{\rm MS}$, as given by Eqs. (14) and (20), underestimates the true extent of the trapped cloud when the MOT is near the boundary between regimes, so that when $r_{\rm MS} = r_l$ about half the atoms will be in the diffuse ball extending out beyond r_l. At low numbers of atoms the trap can also pass directly from the temperature-limited to the two-component regime when $r_T = r_l$.

Equation (21) introduces another numerical factor for which an empirical value is supplied by our experiments (described below). Petrich *et al.* [27] have also recently reported two-component density distributions in a trap working at high magnetic field gradient and high detuning. We find that our model reproduces the position of the boundary between the multiple scattering and two-component regimes in their results (taken at higher laser beam intensities) as well as in our own.

D. Summary

Let us now summarize our understanding of the steady-state MOT. For the range of behavior considered in this paper, the cloud of atoms in a MOT is a physical system described by four parameters. The parameters are the laser Rabi frequency Ω, detuning δ, magnetic field gradient b, and number of trapped atoms N. A useful parameter derived from these is the light shift Ω^2/δ, since this appears in the formulas for temperature [Eq. (12)], density [Eq. (15)], and sub-Doppler capture range [Eq. (21)].

The temperature and confinement at the center of the trap are determined by polarization-gradient forces and by multiple scattering of photons between atoms. In special conditions, the density can be limited by the temperature and the number of atoms, but this is rare; usually the density is limited by multiple scattering and is independent of N. The spatial distribution of the atoms also changes when the trap passes from the temperature-limited to multiple scattering regimes, but experimentally we find that the cloud departs from its Gaussian shape well after the density has already become independent of N (as more and more atoms are loaded). In other words, a Gaussian profile is *not* in itself a sign that the cloud is temperature limited. Multiple scattering of photons also raises the temperature, the excess heating being proportional to $N^{1/3}$. A combination of high magnetic field gradient and small light shift, or else a sufficiently high number of trapped atoms, will cause the trapped cloud to spill outside the central strongly confining region of the MOT, leading to a two-component density distribution and the eventual disappearance of sub-Doppler temperatures. The three regimes we have discussed are summarized in Table II.

The equations for the curves shown in the phase diagrams of Fig. 1 are given in the Appendix.

E. Limitations of the model

There are two important limitations of our model. The first is its failure to consider in detail the behavior when the cloud of atoms becomes optically thick, even though the search for high densities may tend to put the MOT into this regime. The effect of increasing optical thickness is taken into account to some extent, however, by our empirical formula for the density in the multiple scattering regime. The second limitation of the model is the inevitable breakdown of the sub-Doppler cooling and compression processes at low light shifts. This breakdown will be considered as we discuss our experimental results.

Note that although we have talked of a phase diagram for the MOT, we are only using this thermodynamic concept in a very loose way. The closed thermodynamic system present in a MOT is not the trapped cloud of atoms, but the combination of the atoms and the radiation field. The boundaries indicated in Fig. 1 do not define sharp transitions from one behavior to another; the changes are smooth. For example, when the cloud fills up the central sub-Doppler region and approaches the two-component regime, the confining force is not a linear function of position, so that the value of df/dz, when averaged across the radius of the cloud, will produce an "average spring constant" *smaller* than the value predicted by Eq. (11), thereby hastening the onset of the two-component regime.

III. TIME-DEPENDENT MOT

In the preceding section, we have given a steady-state description of the MOT with four independent parameters: the number of trapped atoms N, the field gradient b, the laser Rabi frequency Ω, and detuning δ. Experimentally, the maximal number of atoms N in a steady state is determined by a balance between the capture rate R and losses due to either collisions with room-temperature atoms in the background gas of the vacuum chamber, or

TABLE II. The various regimes of the MOT. The radii $r_T, r_{\rm MS}$, and r_l are defined in Eqs. (8), (20), and (21), respectively.

Small N	$r_{\rm MS} < r_T < r_l$	$n \propto N$, r independent of N
Medium N	$r_T < r_{\rm MS} < r_l$	n independent of N, $r \propto N^{1/3}$
Large N	$r_l <$ greater of $\{r_T, r_{\rm MS}\}$	two-component density distribution

collisions between trapped atoms.

In order to reach the highest densities it is often convenient to work in a transient way. The trap is loaded at parameters b_1, Ω_1, δ_1 leading to the highest steady-state number N_1 of trapped atoms, and is then switched rapidly to new values b_2, Ω_2, δ_2 which, according to the analysis of the preceding section, lead to a higher density. However, since the trap is now being operated in a transient way, it is not clear that the previous treatment, which was a stationary analysis, is still valid. Indeed, the number of trapped atoms will not remain equal to N_1, but will tend to a new value N_2 which is much smaller than N_1, since the conditions which maximize the number are no longer met. We need to determine whether the conclusions of Sec. II remain of interest.

When the trap parameters b, Ω, δ are changed with N kept constant, the atomic cloud relaxes to a new equilibrium shape, with a new density at the center $n(0)$. The time constant for reaching the new value for $n(0)$ is of the order of $\tau_{\rm pos}/3 \simeq 10\,{\rm ms}$, where $\tau_{\rm pos}$ is the relaxation time for an atom initially displaced away from the trap center to move back towards $r = 0$. The calculation of $n(0)$ using the previous analysis will be valid if the number of atoms has not varied significantly during this relaxation time $\tau_{\rm pos}/3$. Indeed, in this case we can consider $N(t)$ as the slow variable of the problem, and the state of the trap adjusts adiabatically as N decreases.

Two time scales enter into the evolution of $N(t)$. The first is the lifetime associated with collisions with background gas atoms; this lifetime is longer than 1 s for the pressures used in our experiments. It is therefore always much longer than the position relaxation time. The second time scale is related to collisions between trapped atoms, and can be quite short if the density is high. This time scale can be estimated as $1/\beta n(0)$, where the loss rate coefficient β for cesium is in the range 10^{-11}–10^{-10} ${\rm cm^3\,s^{-1}}$ [28]. For densities at the center not exceeding a few 10^{11} ${\rm cm^{-3}}$, as found in our experiments, this second time scale is also larger than the position relaxation time $\tau_{\rm pos}/3$. It is, therefore, a good approximation to consider the time-dependent MOT as a quasistatic system evolving to a new equilibrium, its state being described at any time as a particular equilibrium state studied in Sec. II.

IV. EXPERIMENTS

A. Experimental setups

We performed numerous measurements of the spatial density in three separate magneto-optical traps, and of the temperature in one of them. We considered the possibility that the density in a MOT is unexpectedly sensitive to the quality of the alignment, spatial profile, and polarization of the laser beams. This is why we pursued our investigation on three independent traps, one of them in Oxford, and two in Paris. We will label these three traps, in what follows, as traps A, B, and C, respectively. For all the traps the basic geometry was of three mutually perpendicular beam pairs, intersecting at the zero of a quadrupole magnetic field produced by two coaxial coils. Each beam was circularly polarized, those in each pair having opposite polarizations.

Trap A was formed in a large stainless steel vacuum chamber pumped by a diffusion pump and liquid-nitrogen-cooled shield. The trapping light was spatially filtered using single-mode optical fibers. Light from one fiber was split to produce two horizontal trapping beams; light from a second fiber produced a vertical beam. Each beam was retroreflected outside the vacuum chamber (angular alignment to better than $3 \times 10^{-5}\,{\rm rad}$). On a single pass through the chamber, deviations from perfect Gaussian profiles typically consisted of 10% fluctuations in the intensity, with a spatial period of a few hundred micrometers. The chamber windows were antireflection coated and of high optical quality. Two different methods were employed to load the trap, enabling a wide range of steady-state trap numbers and background pressures to be attained. The first method was to capture from a background vapor of a few $10^{-8}\,{\rm mbar}$. This typically loaded 10^7–10^8 atoms, with trap lifetimes in the range 0.25–3 s. The intensity imbalance due to absorption by the background cesium vapor was typically 15%, and was removed by slightly converging the beams. The second method was to load from an unslowed thermal cesium atomic beam. With this method, background pressures down to a few $10^{-9}\,{\rm mbar}$ could be reached, reducing trapping beam imbalances to a few percent. Steady-state trap numbers could be varied in the range 10^4–10^7 by changing the flux of atoms in the beam.

Trap B was formed in a glass cell pumped by a 25 l/s ion pump, which produced a pressure $< 3 \times 10^{-9}\,{\rm mbar}$. The trap was loaded from a second magneto-optical trap about 60 cm above it, housed in another chamber of the same vacuum system. The upper trap collected atoms from a cesium vapor at a pressure $\sim 3 \times 10^{-8}\,{\rm mbar}$ for 2 s. The collected atoms were then cooled to $3\,\mu{\rm K}$ and allowed to drop through a tube down to the lower trap, where they were caught. About 20% of the atoms collected in the upper trap could be transferred to the lower trap in this way. The lower trap (our trap B) was formed using retroreflected laser beams; the walls of the glass cell were not antireflection coated and were not of good optical quality; neither were the beams spatially filtered.

Trap C was formed in a glass cell pumped by a 25 l/s ion pump. The cell was roughly spherical with six flat regions (uncoated) to form windows for the trapping beams. The trapping light was spatially filtered and divided into six independent beams before being passed into the cell. The background gas in the cell was predominantly cesium at a presure of a few $10^{-8}\,{\rm mbar}$; the trap captured slow atoms from this vapor.

We used a calibrated CCD video camera to observe the fluorescence of the trapped cloud of atoms, and in this way measured the radius of the cloud (see Fig. 3). Trap A was observed with two cameras looking simultaneously along the $(1,1,0)$ and $(1,-1,0)$ directions; trap B was observed by a single camera looking along a direction at 20° to the y axis (and occasionally at right angles to this); trap C was observed along the $(0,1,1)$ diagonal. The resolution of the CCD optics was $25\,\mu{\rm m}$ for trap A, and $12\,\mu{\rm m}$ for traps B and C. This was measured by imaging

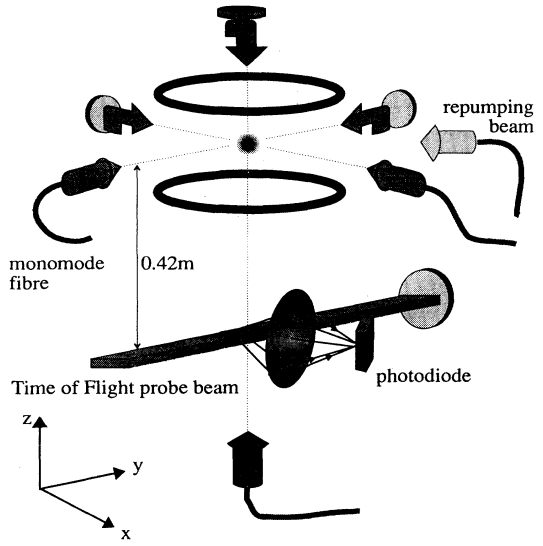

FIG. 3. Experimental setup. Trap A is illustrated, having beams spatially filtered and retroreflected. Not shown are the waveplates and the CCD cameras observing along the $(1,1,0)$ and $(1,-1,0)$ directions.

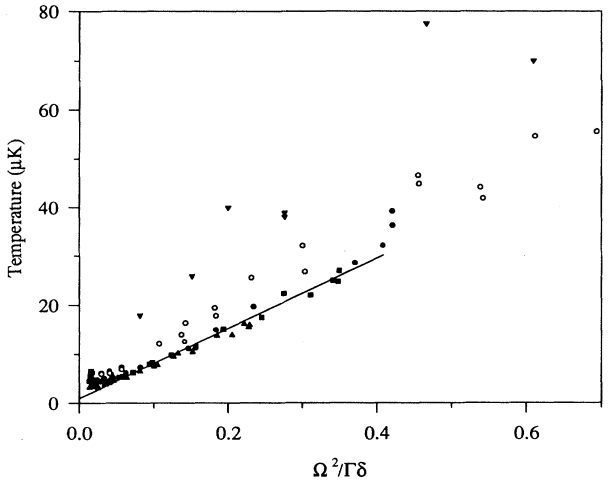

FIG. 4. Temperature measurements on atoms released from a σ^+-σ^- optical molasses made from three mutually perpendicular beam pairs. The symbol shape indicates the detuning as follows: δ/Γ = 1.9(▼), 3.8(○), 5.7(●), 7.6(■), 11.4(▲).

a series of pinholes of various sizes. The finite optical resolution was taken into account when interpreting our measurements.

In all experiments, the light was provided by diode lasers locked to the correct detuning from the cesium resonance using saturated absorption spectroscopy. Each trap had light near resonant with the $6S_{1/2}F = 4 \rightarrow 6P_{3/2}F = 5$ transition in cesium, and repumping light on the $F = 3 \rightarrow F = 4$ transition, to pump atoms out of the lower hyperfine level of the ground state. Since the time-dependent measurements could extend over several seconds, it was important to ensure that the laser detuning was stable to within a MHz on this time scale.

B. Temperature measurements

Temperature measurements on trap A were performed using a time-of-flight (TOF) technique (Fig. 3). To measure molasses temperatures, a small number of atoms, $\sim 5 \times 10^5$, was loaded with the detuning set to $\delta = 2\Gamma$, Rabi frequency $\Omega = 1.5\,\Gamma$, and magnetic field gradient 10 G/cm. The laser parameters $\{\delta, \Omega\}$ were then switched to the required values. After a wait of a few ms the magnetic field gradient was switched off, followed by the light about 10 ms later. The atoms fell down to a standing-wave probe beam positioned 42 cm below the trap and the fluorescence from the probe was recorded as a function of time. At this distance of the probe from the trap, the slight uncertainty in the initial size of the falling cloud of atoms contributed negligibly to the uncertainty in the temperature measurements. The probe beam cross section was 2 cm×2 mm (full width at half maximum).

The results are shown in Fig. 4. We find that when $T < 10\,\mu$K, a linear fit to our results [see Eq. (12)] yields

$$C_0/k_B = 1.9 \pm 0.5\ \mu\text{K}, \quad C_\sigma = 0.24 \pm 0.05 \qquad (0 < T < 10\ \mu\text{K}), \quad (22)$$

in agreement with the results of [4] in this range of temperature. However, in addition, we observe a slight departure from a linear dependence on the light shift. If we force a straight line fit through all our data having $\Omega^2/\Gamma < 0.4$ (i.e., temperatures up to about $30\,\mu$K), we obtain

$$C_0/k_B = 1 \pm 0.5\ \mu\text{K}, \quad C_\sigma = 0.28 \pm 0.05 \qquad (0 < T < 30\ \mu\text{K}). \quad (23)$$

The uncertainty in C_σ is almost entirely due to a 15% uncertainty in the average intensity of the laser field at the position of the trapped cloud.

C. Investigating the fluorescent emission

The total power scattered by an atom can be written $P = \hbar\omega_L \Gamma \Pi^{(e)}$, where $\Pi^{(e)}$ is the total population of all excited states (i.e., all the Zeeman sublevels), assuming these all decay at the same rate Γ, and ω_L is the laser frequency (all the transitions involved have approximately the same frequency). For a two-level atom illuminated by a single traveling wave of Rabi frequency Ω, detuning δ, a textbook calculation yields [22]

$$P = \hbar\omega_L \frac{\Gamma}{2} \frac{\Omega^2/2}{\delta^2 + \Gamma^2/4 + \Omega^2/2}. \quad (24)$$

To calculate the power scattered by a cesium atom in a MOT, on the other hand, one must calculate an average over all the transitions between the various Zeeman sublevels in the ground and excited states. The Rabi frequency and electric field polarization are both complicated functions of position, as is the internal atomic state. The usual way [29] to handle this situation is to assume that the total scattering rate per atom can approximated as

$$P \simeq \hbar\omega_L \frac{\Gamma}{2} \frac{C_1^2\Omega_{\rm tot}^2/2}{\delta^2 + \Gamma^2/4 + C_2^2\Omega_{\rm tot}^2/2}, \tag{25}$$

where $\Omega_{\rm tot}^2$ is determined by the average light intensity in the trap (six times that of any one of the trapping beams), and C_1 and C_2 are average Clebsch-Gordan coefficients. One expects C_1 and C_2 to be of the same order of magnitude, although not necessarily equal.

To measure C_2 we monitored with a photodiode the fluorescent power scattered by atoms in the MOT (a fixed fraction of the total emitted power being imaged onto the diode), while the detuning was suddenly switched between two values. Using Eq. (25) and taking the ratio of the signals for two different values of δ allows C_2 to be deduced knowing $\Omega_{\rm tot}$.

To ensure an accurate measurement, we took into account effects on the beam intensity such as loss during the retroreflection, convergence of the laser beams, and absorption by the trapped cloud. To ensure that conditions in the trapped cloud were reasonably constant, the change in detuning used for the measurements was fairly small; typically a switch from 2Γ to 3Γ was used.

To measure C_1, one possible method is to measure again a change in fluorescent power incident on the photodiode, but this time while all but one of the trapping beams are rapidly switched off (in less than a microsecond), all other conditions being unchanged. The single remaining (circularly polarized) beam quickly optically pumps the atoms into the stretched state $|F = 4, M = 4\rangle$, and one measures the scattered power, now given by Eq. (24), before the atoms are pushed away by this beam. Taking into account the factor of 6 change in the average light intensity, and the value of C_2 already measured, the ratio of the photodiode signals before and after cutting the beams allows C_1 to be deduced. We carried out this procedure for the case of high saturation of the atomic transition, where the signal is large, but our detection was not sufficiently sensitive to enable us to measure C_1 at low saturation.

Our results are shown in Fig. 5. All measurements were done for Rabi frequencies between Γ and 2Γ, and detunings between 2Γ and 3Γ. We found C_1 and C_2 to be equal, within experimental uncertainty: $C_1^2/C_2^2 = 1 \pm 0.25$, and the mean of all the measurements of C_2^2 gave $C_2^2 = 0.73 \pm 0.1$.

At first, one might reason that the light in the three-dimensional interference pattern has all kinds of polarizations at different places, so the value of C_1^2 and C_2^2 must be close to an average for all the transitions and all the polarizations, yielding $C_1^2 \simeq C_2^2 \simeq 0.4$. Our results show that this reasoning is not valid. The measured values indicate that the coupling between the atoms and the radiation field is stronger than a simple average over all possible coupling strengths. This can be explained as arising from optical pumping among the Zeeman sublevels: at any given point in the radiation field the atom is optically pumped towards the state that interacts most strongly with the local field, therefore raising the overall fluorescent scattering rate. This process is at the heart of the Sisyphus effect, which produces the friction in the MOT. In addition, optical potential wells will cause the atoms to spend more time in the regions where their interaction with the light is the strongest, since the light shift of the ground state is most negative for the atomic state having the greatest coupling with the light (for a laser field detuned red of the atomic resonance). Our measurement can, therefore, be interpreted as experimental evidence that one or both of these physical processes is indeed present.

A numerical calculation, using the quantum Monte-Carlo method, for an atom of transition $F = 4 \rightarrow 5$ in a three-dimensional optical molasses of the relevant polarization, yielded an excited-state fraction consistent with $C_1^2 = 0.9 \pm 0.1$, at $\delta = 5\Gamma$, $\Omega = 0.71\Gamma$ [30]. Note that the phase differences between the three standing waves were constant in the calculation, while they are fluctuat-

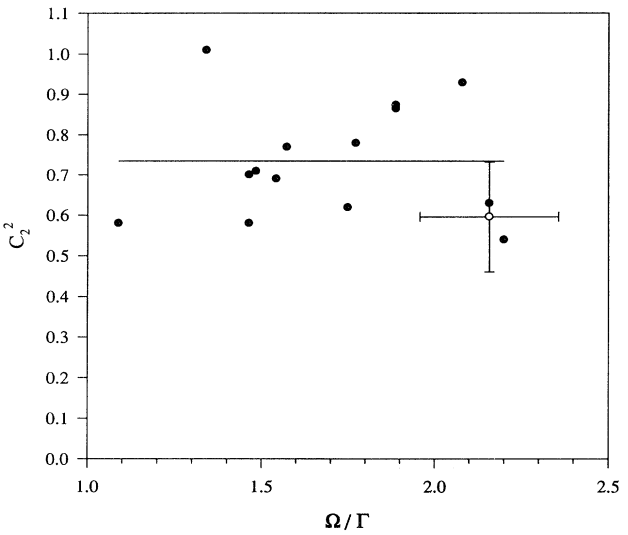

FIG. 5. Squares of the average Clebsch-Gordan coefficients, deduced by the methods described in the text. Filled circles are measurements of C_2^2, the open circle indicates the average of several measurements of C_1^2, with error bars indicating the total uncertainty, which is mainly due to systematic error in the laser intensity at the trap. The C_2^2 value at the same value of Ω/Γ was measured in the same experimental run. The solid line marks the average $C_2^2 = 0.73$. The data represent measurements made over a six month period with numerous different trap alignments and two different trapping beam geometries. The main cause of the scatter is the spatial fluctuation in Rabi frequency at the trap position due to the 5–10% spatial inhomogenities of the retroreflected beam profiles.

ing in the experiment, and the parameter values in the calculation were different from those in the experiments.

To interpret our measurements of number and density in the trap, we took our experimentally measured value of $C_1^2 = 0.7 \pm 0.2$.

D. Measurements of κ

We obtained some information on the value of κ, in order to reduce the present uncertainty illustrated by Table I, and to help in interpreting our density measurements. Our method was to measure the cloud radius for a given temperature and to deduce κ from Eq. (8). However, in order to use this method one must be sure that the trap is indeed in the temperature-limited regime, and so one must use some combination of small number of atoms, low field gradient, low laser intensity and high detuning. These all tend to reduce the intensity of the CCD image of the fluorescence from the trap, and this limited the range of our measurements. With a high beam intensity ($\Omega = 2.2\Gamma$), Fig. 6 shows unambiguously the transition from temperature-limited to multiple scattering limited behavior. We observed the transition equally clearly with other parameter values for trap A, as listed in Table III. At lower beam intensities, however, we never saw a trap unambiguously in the temperature-limited regime. As the trap emptied, the last radius measured before our signal disappeared was always smaller than the previous value (with more atoms loaded), so we could not be sure that the radius did not continue diminishing when even fewer atoms were present. This means that many of our measurements give a lower limit for κ rather than an absolute value. Table III lists our results. To deduce κ from the measured cloud radius, we did not always simultaneously measure the temperature T, but we found that those temperature measurements that we did make were sufficiently reproducible to allow us to regard Fig. 4 as a reliable indicator of T. Each value of the radius and number of atoms in the trap is the average of several measurements; the statistical uncertainties in the radius measurements were about 10%.

As well as providing values for κ, the data in Table III lead us to a deduction. This is that as the number of atoms in the trap increases, the cloud radius starts to increase well before the temperature does. This is shown clearly by Fig. 6 (results for trap A at $\Omega = 2.2\ \Gamma$), and by Table III (results for trap C at $\Omega = \Gamma$). In the former case, multiple scattering has increased the trap volume by a factor of more than 3 when there are 5×10^5 trapped atoms. The study of temperature in [23], on the other hand, implies a temperature increase of less than 10% with this number of atoms. In the latter case, the density remained constant at $\sim 8 \times 10^{10}$ cm^{-3}, for numbers of trapped atoms between between 10^5 and 10^7. This implies that multiple scattering is limiting the density when

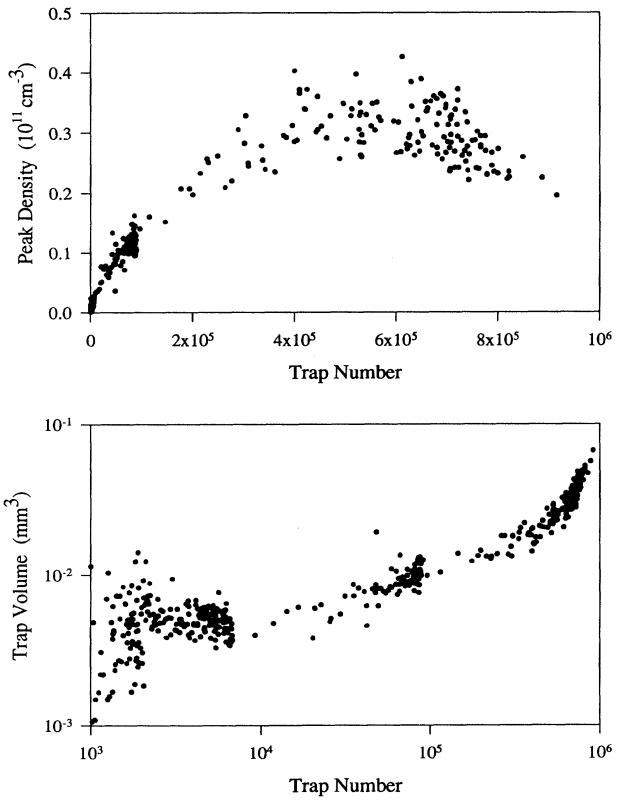

FIG. 6. Trap density and volume versus number. The trap was loaded from an unslowed atomic beam. The trapping parameters were $\delta = -3.4\Gamma$, $\Omega^2 = 4.4\Gamma^2$ per beam, and $dB/dz = 10$ G/cm. The volume quoted is the $1/e$ full width volume. Each point represents an analysis of one field (one half frame) of the video signal obtained while the trap emptied. Three separate experiments with differing initial number of trapped atoms and aperture size on the camera are shown.

TABLE III. Information pertinent to deducing the spring constant κ. In the final columns, the spring constant is calculated by assuming the trap is in the temperature-limited regime and taking the temperature from Fig. 4. When the trap is obviously not in the temperature-limited regime no value is given, and when the trap is close to but not yet temperature limited the value is given in brackets.

Trap	Ω^2/Γ^2	δ/Γ	dB/dz G/cm	$N/10^5$	r μm	κ (10^{-19} N/m)	κ_0
A	0.5	2.8	5		35	1.6	0.9
A	4.9	3.4	10	0.1	50	2.5	0.84
A	5.2	3.4	10	0.1	51	3.5	1.2
A	5.2	3.4	30	0.01	40	5.9	0.7
B	0.87	2.2	58	0.36	23	12	0.44
B	0.87	2.2	31	1	37	(4.7)	(0.33)
C	0.28	3	9.5	2.4	47	(0.95)	–
C	1	5	9.5	1	37	(1.5)	(0.78)
C	1	5	9.5	2.5	49	(0.95)	(0.5)
C	1	5	9.5	30	99	–	–
C	1	5	9.5	100	150	–	–
C	1	5	5	3.5	71	(0.4)	(0.4)

there are as few as $N \sim 10^5$ atoms in the trap, for these parameter values, while the studies of temperature in [4] and [23] both indicate that T increases negligibly with so few atoms. The conclusion for the phase-space density is that multiple scattering limits the phase-space density *first* by limiting the density; the temperature increases only at higher numbers of trapped atoms.

The results in Table III with the smallest N are those that give the most reliable lower limit for κ_0. Therefore, our conclusion is that $\kappa_0 = (1 \pm 0.2) \times 10^{-19}\,\mathrm{Nm}^{-1}$ for trap A, $\kappa_0 > 0.4 \times 10^{-19}\,\mathrm{Nm}^{-1}$ for trap B, $\kappa_0 > 0.8 \times 10^{-19}\,\mathrm{Nm}^{-1}$ for trap C. Our results are inconsistent with the lowest values indicated in Table I. We believe we have avoided the two main problems that can lead to underestimates of κ_0, namely, residual multiple scattering of photons and excursions of the trapped cloud into the nonlinear region of the trapping force.

E. Nonlinearity of the confining force

In this section we discuss measurements on traps A and B, in which we observed the transition between the multiple scattering and two-component regimes. This was done by observing the trap at fairly high magnetic field gradients (up to 60 G/cm).

The characteristic behavior as one passes into the two-component regime was described in Sec. II C and is also reported in [27]. Figure 7(a) shows a sample density distribution of the fluorescing cloud in trap A. This distribution was obtained from a horizontal line of the CCD image of the cloud. It can be fitted by two superposed Gaussians of differing radii and peak density. Note that the ratio of the radii of these two Gaussian distributions can be larger than ten, so that even if the more diffuse Gaussian component has a peak density 100 times smaller than that of the denser component, making it difficult to see on the CCD image, it will nevertheless still contain almost all of the atoms. In Fig. 7(b) we show a time-of-flight signal obtained from trap A under the same conditions as for Fig. 7(a). We observe that the velocity distribution can also be modeled as the superposition of two Gaussians, and we find that the number of atoms in the colder of the two velocity distributions is equal to the number of atoms in the narrower of the two density distributions. This represents experimental evidence that only those atoms confined in the central region of the trap are more efficiently cooled by the sub-Doppler mechanism, as one would expect.

We studied the onset of the two-component regime by loading trap A or B under normal conditions, then simultaneously ramping the laser detuning and magnetic field gradient to some chosen value. The duration of the ramp, about 20 ms, was slow enough compared to $\tau_{\mathrm{pos}}/3$ to allow the atoms to follow, and thus reach the new equilibrium conditions. On the other hand, it was sufficiently fast compared to the characteristic time for loss that only a small reduction in the number of atoms occurred during the ramp. The two-component density distribution appeared only when both the field gradient and detuning were increased above their normal values (15 G/cm, 3 Γ). Indeed, the two component regime appeared just in the expected region of the MOT's phase diagram (Fig. 8). We observed this regularly simply by watching the video image of the fluorescing cloud while the trap parameters

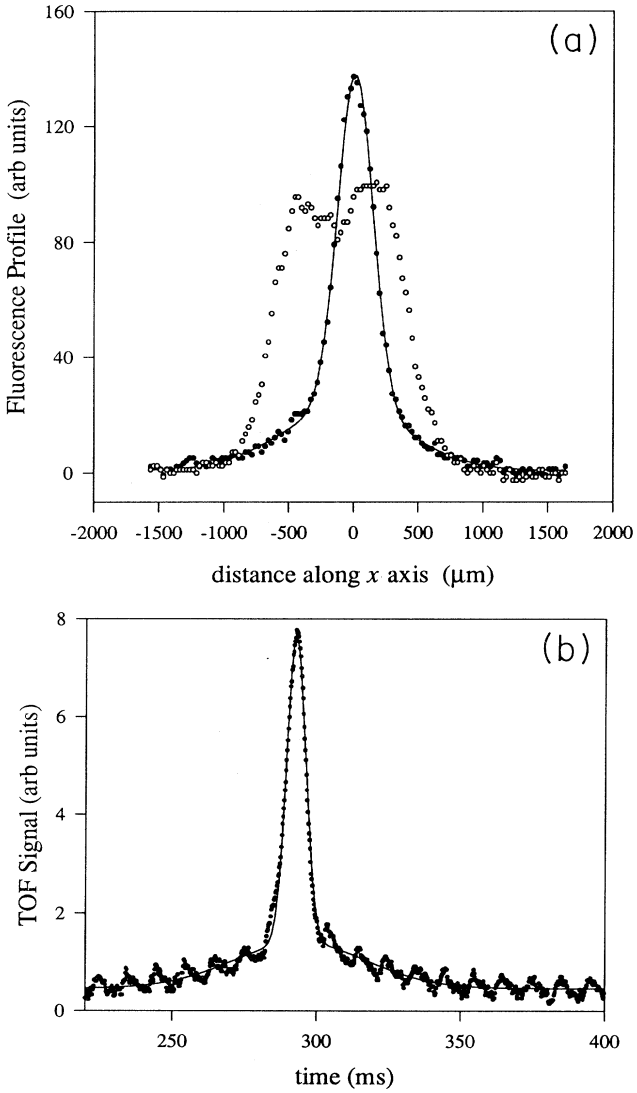

FIG. 7. (a) A horizontal line from the CCD image and (b) the corresponding time-of-flight signal, for trap A, with $\Omega^2 = 0.56\,\Gamma^2$, $\delta = 5.7\,\Gamma$, $N = 2 \times 10^7$ atoms. In (a) the CCD image is shown for two values of the magnetic field gradient: $dB/dz = 10$ G/cm (open symbols, ○) and $dB/dz = 45$ G/cm (filled symbols, ●). The line through the latter signal is a fitted curve consisting of the sum of two Gaussians. In (b) the TOF signal is shown only for the case $dB/dz = 45$ G/cm (points), with a fitted curve which is the sum of two Gaussians (line). The TOF signal at the lower field gradient (not shown) was well fitted by a single Gaussian. We interpret this data as showing an example of the multiple scattering and two-component regimes. For the lower field gradient, the trap is in the multiple scattering regime and has a roughly uniform density distribution. For the higher field gradient, the density and velocity distributions consist of two components, as described in the text.

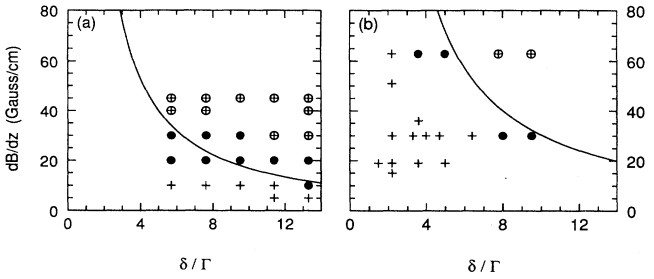

FIG. 8. Parameter values at which density measurements were made. (a) Measurements on trap A, with $\Omega^2 = 0.56\,\Gamma^2$, $N = 2 \times 10^7$ atoms. (b) Measurements on trap B, with $\Omega^2 = 0.8\,\Gamma^2$, $N = 5 \times 10^6$ atoms. The symbol shape indicates whether the observed density distribution consisted of a single narrow component +, two components (⊕) (one narrow, one broad), or an intermediate distribution (•). The density distribution was also observed at other parameter values; the figure indicates only those values for which a careful analysis was carried out. The solid curves in (a) and (b) show the position of the boundary $r_{\rm MS} = r_l$ between the multiple scattering and two-component regimes, as predicted by our model with the empirical values $\kappa_0 C_{\rm MS} = 5 \times 10^{-18}$ N/m (see Sec. IV F) and $C_l = 1.4$ for trap A, $C_l = 1.2$ for trap B.

were changed. In addition, we carried out a detailed program of data acquisition and analysis for a subset of all the possible parameter values. The values at which precise measurements were made are indicated in Figs. 8(a) (trap A) and 8(b) (trap B).

Figure 9 shows the density at the center of the trap,

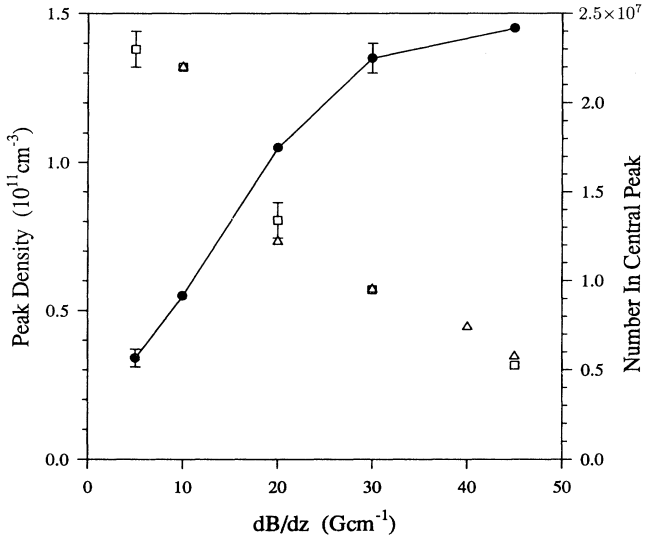

FIG. 9. Density at the center of the cloud (•) and number of atoms in the central component (open symbols) as a function of magnetic field gradient, in the two-component regime. The laser parameters were $\Omega^2 = 0.56\,\Gamma^2$, $\delta = 5.7\,\Gamma$. The open squares show the number in the *central* component of the *density* distribution, as deduced from the CCD signal, while the triangles show the number in the *cold* component of the *velocity* distribution, as deduced from the TOF signal. The fact that these two numbers agree is evidence that the colder atoms originate from the central part of the cloud.

and the number of atoms in the central component of the density and velocity distributions, as a function of magnetic field gradient. Our model predicts a density proportional to field gradient if the atoms are in a regime limited by multiple diffusion inside the sphere with radius r_l. This is only observed for field gradients up to about 30 G/cm. At the higher magnetic field gradients the scaling law suggested by the model clearly no longer applies. This may be due to a breakdown of the static model at high field gradients caused by large collisional loss rates (Sec. III). The results imply that a useful increase in the density is only obtained for field gradients easily produced in the lab, less than 100 G/cm.

The results in Fig. 9 for the number of atoms in the central peak show the expected falloff as the magnetic field gradient is increased. The reduction is not as rapid as predicted for a MOT in the two-component regime, however. The observed number follows a law approximately $\propto b^{-1}$ (the inverse of the field gradient), rather than $\propto b^{-2}$ [Eq. (A4)]. We interpret this as the behavior in the transition region between the multiple scattering and two-component regimes. The observed radius of the central peak in this transition region varies roughly as $b^{-0.6}$.

For a MOT well into the two-component regime, we expect the radius of the central component of the density distribution to be roughly equal to the radius r_l of the sub-Doppler region of the MOT [Fig. 2, Eq. (21)], and therefore to scale as b^{-1}, not $b^{-0.6}$. By using only measurements when the MOT is certainly well into the two-component regime, and not close to the boundary between regimes, we find results consistent with Eq. (21), although the restricted set of data points (see Fig. 8) is now not large enough to confirm this equation unambiguously. At a field gradient of 40 G/cm in trap A, the radius of the central component was 84 μm and 64 μm for detunings 8.6 Γ and 11.4 Γ, respectively, at $\Omega = 0.75\,\Gamma$. These figures are consistent with $r_l \propto 1/\delta$, and imply $C_l = 1.4 \pm 0.3$. Closer to the boundary between regimes, the radius of the central component varied more slowly with δ. In trap B with a field gradient $b = 62$ G/cm, the radius of the central component was 45 μm at $\delta = 9.5\,\Gamma$, $\Omega = 0.9\,\Gamma$; these figures imply $C_l = 1.2 \pm 0.3$.

F. Density measurements

We measured the density at numerous different points in parameter space (see Fig. 8), each density value being the average of between 3 and 10 measurements. To measure the spatial density of atoms in the trap, we used two related methods. The first was to measure the total number of trapped atoms and deduce the density using the cloud radius already measured, $n \propto N/r^3$. The total number of atoms was deduced by measuring the power of the fluorescent light emitted into a known solid angle with a photodiode. This relies on one knowing the formula for how much light is emitted per atom for a given incident laser-beam intensity and detuning — for this we used our measurements of the relevent Clebsh-Gordan coefficient, described in Sec. IV C. The second method

was to calibrate the light sensitivity of the CCD camera and use just the CCD signal to gain all the required information. Once again, we need to know how much fluorescent power is emitted per atom, but the advantage of this second technique is that it is less sensitive to errors in the measurement of the cloud dimensions. Assuming the cloud is well imaged onto the CCD array, the video signal S is proportional to the integral of the number of atoms along the "line of sight" (see Fig. 10), so the atomic density is deduced using the equation $n \sim S/r$ — the radius no longer appears in the third power. Furthermore, because we no longer average over the whole trap volume, the measurement is much less sensitive to uncertainties in the three-dimensional shape of the density distribution. Finally, our CCD video signal had a better signal-to-noise ratio than our photodiode signal when the atoms' fluorescent power was small.

We have listed several advantages of the second method (Fig. 10) over the first. The one disadvantage is that the second method is more sensitive to lens aberrations in the imaging onto the CCD array. We took special care to ensure that such aberrations were not affecting our measurements. We imaged a glowing tungsten filament onto the CCD array and investigated aberrations in the optics by increasing an aperture fixed to the front of the camera objective. The recorded CCD signal (at the pixels where the filament is imaged) should be proportional to the area of the aperture. For small apertures this is the case, but at larger apertures it is not, even though the *resolution* (indicated by the width of the image) remains almost unaffected. This is because spherical aberration causes off-axis rays to be distributed over a relatively wide area in the image plane. The measurements on the MOT were performed using an aperture of diameter 13 mm on the camera objective, positioned at a distance of 280 mm from the MOT for trap A, and apertures of 12 mm at distances of 120 mm for traps B and C. The CCD sensitivity was calibrated using a laser beam of known intensity (observations on traps B and C), and light imaged from a cesium discharge lamp (observations on trap A). Comparing the total number of atoms in the trap, as deduced from the CCD signal alone, with the number deduced from the photodiode signal alone, provided a consistency check of our calibrations.

We used the video signal to examine the time dependence of the density as well as to look at the steady state. For trap A a part of the video signal was digitized in real time using a fast frame grabbing board. For traps B and C a single horizontal line from the CCD signal was chosen and digitized in real time.

The results of our density measurements on trap B in the regime limited by multiple diffusion are summarized in Fig. 11. We find that the density scales approximately as $b^{0.8}\delta^{0.4}$ for most of the measurements shown. In our model we chose to approximate this dependence by the simpler scaling law of Eq. (14). A least-squares fit of Eq. (14) to the observations gives the value

$$C_{\mathrm{MS}}\kappa_0 = (5 \pm 1) \times 10^{-18}\ \mathrm{N/m}. \tag{26}$$

Taking $\kappa_0 = (1 \pm 0.5) \times 10^{-19}\,\mathrm{N/m}$ (see Sec. IV D), this implies $C_{\mathrm{MS}} = 50 \pm 25$ for trap B.

Measurements at lower intensity ($\Omega^2 = 0.56\,\Gamma^2$) in trap A are shown in Fig. 12. We find that when the detuning is above about six atomic linewidths, the density begins to *decrease* with detuning, so the scaling law $n_{\mathrm{MS}} \propto \delta^{0.4}$ is no longer obeyed. We interpret this as evidence of a limitation on the confinement at the center of the MOT for low values of the light shift Ω^2/δ. Our results suggest that at low light shift, not only is the capture range of the compressive force reduced (putting the MOT in the two-component regime), but also the confinement at the center of the trap is less efficient. This confinement is produced by a balance between the restoring force associated with the spring constant κ and multiple scattering processes which limit the density. Our results could be explained in terms of a reduction in the spring constant within the central region of the MOT. This would be in agreement with the findings in [5], in which measurements of such a reduction were presented. However,

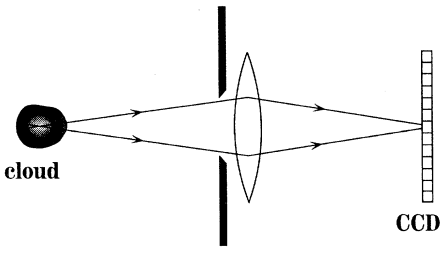

FIG. 10. Density measurement technique. By precisely imaging the trap fluoresence, using a small aperture to avoid spherical aberration, a CCD signal is obtained, at each pixel, which is proportional to the integral of the atomic density along a single line through the fluorescing cloud.

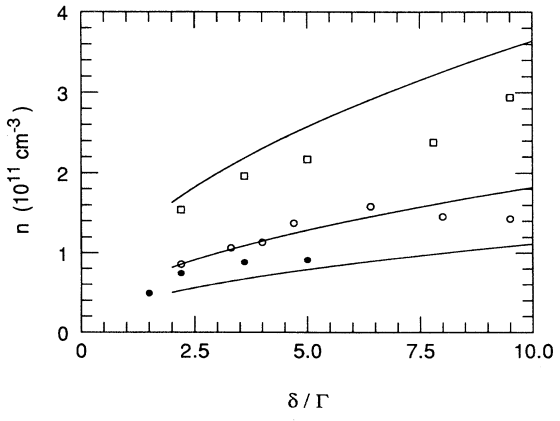

FIG. 11. Density measurements in trap B, with $\Omega^2 = 0.8\,\Gamma^2$, $N = 5 \times 10^5$. The symbols indicate the magnetic field gradient dB/dz = 19 G/cm (●), 31 G/cm (○), and 60 G/cm (□). The lines are the model prediction, using $C_{\mathrm{MS}}\,\kappa_0 = 5 \times 10^{-18}$ N/m.

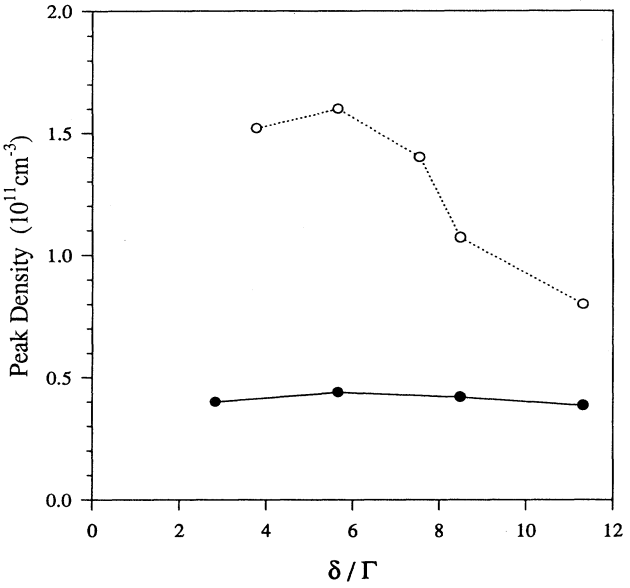

FIG. 12. Density measurements in trap A. $dB/dz = 10$ G/cm, and the symbol shape indicates $\Omega^2 = 4.4\,\Gamma^2$ (●) and $2.3\,\Gamma^2$ (○).

in the previous work it was not possible to ascertain whether or not the reduction was because the MOT was entering the two-component regime and so experiencing a reduced average restoring force or whether, as our own results suggest, the confinement process was vanishing completely.

The results at $\delta = 6\,\Gamma$ in Fig. 12 can be used to deduce the parameters in the model for trap A. We find

$$C_{\rm MS}\kappa_0 = (4 \pm 1.5) \times 10^{-18}\,{\rm N/m}, \tag{27}$$

where the large error bar is because the result is based on fewer measurements than for trap B. The result is consistent with the one we obtained for trap B, so the two traps were producing similar densities in similar circumstances. Using $\kappa_0 = (1 \pm 0.2) \times 10^{-19}\,{\rm N/m}$, which is the value we measured for trap A (see Sec. IV D), we deduce $C_{\rm MS} = 40 \pm 20$.

Density measurements for trap C are listed in Table IV. The final column gives the deduced value for $C_{\rm MS}\,\kappa_0$. The spread in the values of $C_{\rm MS}\,\kappa_0$ indicates the statistical error, which was larger in trap C than in the other traps because we only imaged the cloud from one direction rather than from two perpendicular directions. We obtain

$$C_{\rm MS}\kappa_0 = (12 \pm 3) \times 10^{-18}\,{\rm N/m}. \tag{28}$$

This value is 2.4 times larger than that obtained in the other two traps. That is, trap C produced clouds about two and a half times denser than those in the other traps under the same conditions. The main difference in the optical setup of trap C was that it was composed of six independent laser beams, while the other two traps used three retroreflected laser beams. We think that the higher densities observed in trap C demonstrate that the independent-beam setup gives improved confinement. This could be because the refraction and diffraction of the trapping beams by the cloud of atoms in the MOT changes the retroreflected traveling wave sufficiently to halve the confining force on the atoms.

TABLE IV. Density measurements in trap C. The final column shows the phase-space density, assuming that the temperature was equal to the relevent value indicated in Fig. 4.

Ω^2	δ	dB/dz	n	$\kappa_0 C_{\rm MS}$	ρ
Γ^2	Γ	G/cm	10^{11} atoms/cm^3	10^{-18} N/m	10^{-5}
1	5	5	0.5	13	0.3
1	5	9	0.8	12	0.5
0.3	5	5	1.1	16	1.7
0.3	3	9	0.9	9.5	1.0
0.3	3	14	1.5	10	1.6

G. Comparison with previous work

Many authors have reported densities in a magneto-optical trap of the order of several times 10^{10} atoms per cm^3. This is for traps under conditions normal for loading. There are not many reported measurements of compressed traps. Measurements at high magnetic field gradients were reported in [27], with results of order 2×10^{11} atoms per cm^3, in broad agreement with our own findings. A set of careful measurements is reported in [4], on the other hand, which is *not* in agreement with our results. In this work a MOT made from six independent beams was used and so is comparable with our trap C. At low laser intensities ($\Omega^2 < 0.5\,\Gamma^2$) the densities reported in [4] are from 4 to 6.5 times higher than those we measure under comparable circumstances in trap C. At higher intensities, $\Omega^2 \sim \Gamma^2$, the density reported in [4] is more than 20 times higher than our results. It is not clear how to explain such a large discrepancy. We believe it may be due to a high sensitivity of the MOT in the multiple scattering regime to the quality of the laser beams, especially when the laser field saturates the atomic transition. The MOT is much more sensitive to imbalances between the laser beams (caused by irregularities in the beam profile for example) when the atoms are saturated, since the restoring force at the edge of the trapped cloud is then of the same order as the scattering force that would be exerted by each laser beam acting alone. At low saturation, on the other hand, the restoring force is produced by the sub-Doppler process related to the polarization gradient, and this force is relatively insensitive to imbalances between the traveling waves [3,25]. We suggest that the factor ~ 5 difference between our measurements at low light intensity and those previously reported may, nevertheless, be explainable in terms of the trapping beam quality. The factor 2.4 difference that we ourselves observed between different traps suggests this line of reasoning. We hope to elucidate this in future research with an improved optical setup.

H. Density in phase space

Figure 13 shows the results of measurements in trap A in which both the density and the temperature of the cloud were measured. We observed a phase-space density of $\rho = (1.1 \pm 0.2) \times 10^{-5}$ with a magnetic field gradient of 40 G/cm, $\Omega^2 = 0.5\,\Gamma^2$ and $\delta = 7.6\,\Gamma$. This is the value of the phase-space density at the peak of a Gaussian distribution of atomic position and velocity. There were $N \simeq 3 \times 10^6$ atoms in this Gaussian distribution (a small fraction of the total number of atoms in the trap).

Since trap C produced higher spatial densities than the other traps, we believe it also produced higher phase-space densities, although we did not measure the temperature in this trap. We argue that the temperature in the MOT is reliably indicated by Fig. 4 (which agrees with previous work [4]), so we can assume the temperature in trap C was equal to the value indicated by Fig. 4 for the relevent light shift and detuning, as long as the field gradient and number of atoms in the trap were not too high (below 20 G/cm and 10^6 atoms, respectively). Using this assumption, the final column of Table IV indicates the phase-space density in trap C. We find $\rho = (1.6 \pm 0.5) \times 10^{-5}$ at $b = 14$ G/cm, $\Omega^2 = 0.3\,\Gamma^2$, $\delta = 3\,\Gamma$.

Figure 14 shows a graph of the density in phase space in trap A as a function of light shift, normalized to a field gradient of 30 G/cm. All our density measurements are plotted, and in the case where the density was measured at a field gradient b other than 30 G/cm, the result has been rescaled by $(30b_0/b)^{0.8}$ to obtain the normalized value. Figure 14 indicates that at high light shifts the density in phase space ρ increases as the light shift decreases, but ρ reaches a limiting value of about $(1.5 \pm 0.5) \times 10^{-5}$ at $\Omega^2/\delta \simeq 0.1\,\Gamma$. Our discussion above has shown that this limitation occurs because of a reduction of the confinement in the trap in the multiple scattering regime at low light shifts, which causes the spatial density to decrease. The density in phase space thus reaches a maximum value even though the temperature continues to decrease at lower light shifts (see Fig. 4).

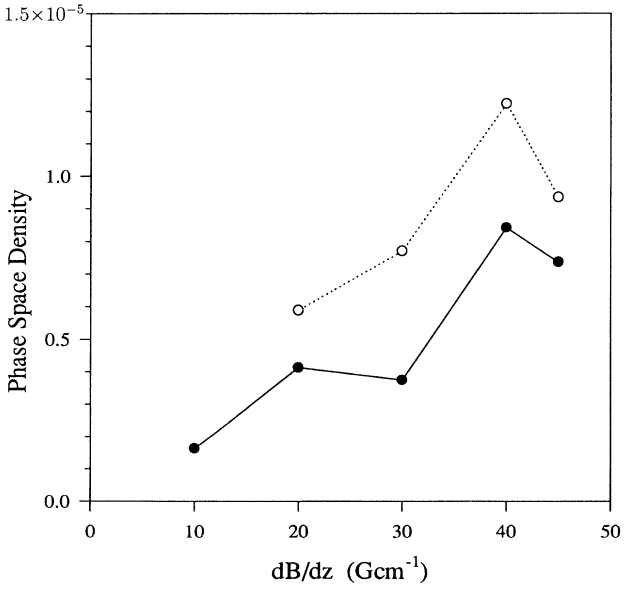

FIG. 13. Phase-space density [Eq. (2)] in trap A. Measurements of the density and temperature of the central component of the phase-space distribution are combined. For this data, $\Omega^2 = 0.5\,\Gamma^2$, and the symbols indicate $\delta = 5.7\,\Gamma$ (●) and $7.6\,\Gamma$ (○).

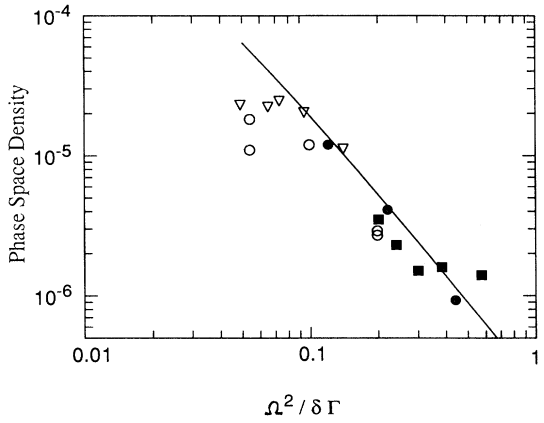

FIG. 14. Phase-space density [Eq. (2)] in trap A as a function of the light shift, normalized to $b = 30$ G/cm. The symbols are as follows: $\Omega^2/\Gamma^2 = 0.56$(▽), 0.6(○), 1.3(●), 2.3(□). The line is the prediction of the model, using $C_{\rm MS}\,\kappa_0 = 4 \times 10^{-18}$ N/m.

V. CONCLUSION

In summary, we have presented an empirical model of the magneto-optical trap which is a useful guide to identifying how the trap will behave under a variety of experimental conditions. The model helps us identify which experimental conditions lead to the highest phase-space densities in the trap. The model is based on a large number of experimental findings, which we have presented.

We measured the temperature in the optical molasses obtained after the magnetic field of the MOT was turned off, for a range of values of the laser detuning and intensity. We find temperatures in agreement with previous studies.

We measured the radius of the cloud of atoms trapped in the MOT when the number of trapped atoms was low. This enabled us to deduce the spring constant κ for one of our traps (trap A) when the laser beam intensity was fairly high and enabled us to obtain lower limits for the spring constant in the other two traps. There is a range of about a factor 10 in previously reported measurements of κ (shown in Table I); our value is towards the upper end of this range. These measurements lead to a value

for κ_0, the first of three parameters in our model.

Our model predicts that when sufficient atoms are loaded into the MOT, the distribution in position and in velocity will consist of a dense, cold, central part, surrounded by a relatively diffuse and hot part. This limits the *number* of atoms that can be confined at high phase-space density. We have observed this effect under a variety of experimental conditions and confirmed the qualitative description provided by the model. Our observations include measurements of the distribution of atomic velocity as well as position. They lead to a value for C_l, the second parameter of the model.

We have measured the density in three different MOT's, under a range of conditions, and deduced the third parameter $C_{\rm MS}$ in our model. We find that the maximum density in the MOT varies much more slowly with laser detuning and intensity than one would expect on the basis of a very simple model of multiple scattering of photons in the trapped cloud.

We find that the multiple scattering process limits the phase-space density mainly by its influence on the spatial density of the atoms, rather than by increasing the temperature. The phase-space density reaches a maximum value when the light shift parameter $\Omega^2/\delta\Gamma$ is decreased to around 0.1. This phase-space limit is caused by a reduction of the spatial density, rather than an increase of the temperature. It indicates that the confinement process in the MOT breaks down before the sub-Doppler cooling mechanism does.

We have obtained evidence that the maximum density one can obtain in a MOT depends significantly on the exact optical arrangement used to construct the MOT. Two of the three different MOT's we examined used a geometry consisting of three retroreflected laser beams, while the third used six laser beams divided outside the vacuum system and directed independently to form the three standing waves of the MOT. While the first two traps gave similar densities, the third gave densities 2.4 times higher under equivalent conditions.

The highest phase-space densities we have observed are of the order of $\rho = n\Lambda^3 = 1.5 \times 10^{-5}$. This is about a factor of 10 below the values reported in [4], a fact which we have not been able to explain satisfactorily. However, we believe it may be due to a difference in the quality of the optics used to create the MOT.

The densities we have observed were small enough that we could consider the MOT to be in quasiequilibrium at any time, even in its compressed phase. However, a factor of 10 increase in the density would bring the MOT into the regime where the dynamics due to cold collisions will be as fast as the equilibration time for atomic position. These collisions would then be the limiting factor on the density achievable in a compressed MOT.

ACKNOWLEDGMENTS

We would like to acknowledge helpful discussions with C. Salomon, A. Clairon, and K. Mølmer. This work was supported by EPSRC, DRET, CNRS, Collège de France and DRED. A.M.S. was financed by the Commission of the European Communities through a Community training project, and by the Royal Society.

APPENDIX

Here we bring together various equations delineating the various regions of the trap.

The boundary between the temperature-limited and multiple scattering regimes is defined by $r_T = r_{\rm MS}$. We can express this as an equation for the number of trapped atoms when the cloud just reaches this boundary. Using Eqs. (8) and (20), which define the two radii, we obtain

$$N = n_{\rm MS}\left(\frac{2\pi k_B T}{\kappa}\right)^{3/2}. \tag{A1}$$

The same condition $r_T = r_{\rm MS}$ can also be expressed as a formula for the field gradient in terms of the other parameters:

$$\frac{b}{b_0} = \frac{\delta}{\Gamma}\frac{1}{\kappa_0}\left(\frac{n_{\rm MS}}{\kappa N}\right)^2 (2\pi k_B T)^3 \tag{A2}$$

This equation is used in Fig. 1.

The boundary between the mutiple scattering and two-component regimes is defined by $r_{\rm MS} = r_l$. Using the defining Eqs. (20) and (21), we find that the number of trapped atoms when the cloud enters the two-component regime is

$$N = \left(\frac{\hbar\Gamma}{\mu_B b_0}\right)^3 n_{\rm MS}\left(\sqrt{2\pi}\,C_l\right)^3\left(\frac{\Omega^2}{\delta\Gamma}\frac{b_0}{b}\right)^3. \tag{A3}$$

In the limit $\delta \gg \Omega, \Gamma$, the number fulfilling the boundary condition scales as

$$N \sim \left(\frac{\Omega^2}{\delta\Gamma}\right)^{5/2}\frac{1}{b^2}. \tag{A4}$$

The condition $r_{\rm MS} = r_l$ can also be expressed as a formula for the field gradient, as follows:

$$\frac{b}{b_0} = \left(\frac{\sqrt{2\pi}\,C_l\hbar\Gamma}{\mu_B b_0}\right)^{3/2}\left(\frac{C_{\rm MS}\kappa_0}{\lambda\hbar\Gamma N}\right)^{1/2}\left(\frac{\Omega^2}{\delta\Gamma}\right)^{5/4}. \tag{A5}$$

This is used in Figs. 1 and 8.

Finally, the boundary $r_T = r_l$ between the temperature-limited and two-component regimes (which becomes important at low Ω, high δ) is given by

$$\frac{b}{b_0} = \left(\frac{\hbar\Gamma}{\mu_B b_0}\right)^2\frac{\Omega^4}{\delta^3\Gamma}\frac{C_l^2\kappa_0}{k_B T}. \tag{A6}$$

[1] E. L. Raab *et al.*, Phys. Rev. Lett. **59**, 2631 (1987).
[2] J. Opt. Soc. Am. B **6** (1989) (see feature on laser cooling and trapping of atoms).
[3] A. M. Steane, M. Chowdhury, and C. J. Foot, J. Opt. Soc. Am. B **9**, 2142 (1992).
[4] M. Drewsen *et al.*, Appl. Phys. B **59**, 283 (1994).
[5] C. D. Wallace *et al.*, J. Opt. Soc. Am. B **11**, 703 (1994).
[6] P. Kohns *et al.*, Europhys. Lett. **22**, 517 (1993).
[7] A. Höpe *et al.*, Europhys. Lett. **22**, 669 (1993).
[8] K. Ellinger, J. Cooper, and P. Zoller, Phys. Rev. A **49**, 3909 (1994).
[9] K. Lindquist, M. Stephens, and C. Wieman, Phys. Rev. A **46**, 4082 (1992).
[10] W. Ketterle *et al.*, Phys. Rev. Lett. **70**, 2253 (1993).
[11] M. H. Anderson, W. Petrich, J. R. Ensher, and E. A. Cornell, Phys. Rev. A **50**, R3597 (1994).
[12] A. M. Steane and C. J. Foot, Europhys. Lett. **14**, 231 (1991).
[13] T. Walker, D. Sesko, and C. Wieman, Phys. Rev. Lett. **64**, 408 (1990).
[14] D. W. Sesko, T. G. Walker, and C. E. Wieman, J. Opt. Soc. Am. B **8**, 946 (1991).
[15] G. Hillenbrand, C. J. Foot, and K. Burnett, Phys. Rev. A **50**, 1479 (1994).
[16] G. Hillenbrand, K. Burnett, and C. Foot (unpublished).
[17] A. Hemmerich and T. W. Hänsch, Phys. Rev. Lett. **68**, 1492 (1992).
[18] R. J. Rafac *et al.*, Phys. Rev. A **50**, R1976 (1994).
[19] C. Salomon (private communication).
[20] C. Salomon *et al.*, Europhys. Lett. **12**, 683 (1990).
[21] Y. Castin and K. Mølmer, Phys. Rev. Lett. **74**, 3772 (1995).
[22] C. Cohen-Tannoudji, J. Dupont-Roc, and G. Grynberg, *Atom-Photon Interactions* (Wiley, New York, 1992).
[23] C. J. Cooper *et al.*, Europhys. Lett. **28**, 397 (1994).
[24] A. M. Steane, G. Hillenbrand, and C. J. Foot, J. Phys. B **25**, 4721 (1992).
[25] J. Werner, H. Wallis, G. Hillenbrand, and A. Steane, J. Phys. B **26**, 3063 (1993).
[26] K. Mølmer (private communication).
[27] W. Petrich, M. H. Anderson, J. R. Ensher, and E. A. Cornell, J. Opt. Soc. Am. B **11**, 1332 (1994).
[28] D. Sesko *et al.*, Phys. Rev. Lett. **69**, 961 (1989).
[29] P. D. Lett *et al.*, J. Opt. Soc. Am. B **6**, 2084 (1989).
[30] Y. Castin (private communication).